Supporting Information for "Role of Collector Alternating Charged Patches on Transport of *Cryptosporidium parvum* Oocysts in a Patchwise Charged Heterogeneous Micromodel"

Environmental Science and Technology

Feb. 2013

Yuanyuan Liu[1], Changyong Zhang[2], Dehong Hu[2], Mark S. Kuhlenschmidt[3], Theresa B. Kuhlenschmidt[3], Steven E. Mylon[4], Rong Kong[5], Rohit Bhargava[5], Thanh H. Nguyen[1*]

[1]Department of Civil and Environmental Engineering, the Center of Advanced Materials for the Purification of Water with Systems,
University of Illinois at Urbana-Champaign, Urbana IL 61801

[2]Fundamental and Computational Sciences Directorate
Pacific Northwest National Laboratory, Richland WA 99354

[3]Department of Pathobiology
University of Illinois at Urbana-Champaign, Urbana IL 61801

[4]Department of Chemistry, Lafayette College, Easton PA 18042

[5]Department of Bioengineering, Micro and Nanotechnology Laboratory and Beckman Institute for Advanced Science and Technology,
University of Illinois at Urbana-Champaign, Urbana IL 61801

[*]Corresponding author phone: (217)244-5965; fax: (217)333-6968; e-mail: thn@illinois.edu

E-mails of authors: liu40@illinois.edu, Changyong.Zhang@pnl.gov, Dehong.Hu@pnl.gov, kuhlensc@illinois.edu, tkuhlens@illinois.edu, mylons@lafayette.edu, rkong3@illinois.edu, rxb@illinois.edu, thn@illinois.edu

Materials and Reagents. The silicon wafer was purchased from Virginia Semiconductor (100 mm in diameter and 0.5 mm in thickness). The Fe_2O_3 source was purchased from Kurt J Lesker (99.9% Fe_2O_3). Photoresist polymer (PR, AZ 4620), PR developer (AZ 400K), and PR stripper (AZ 400 T) were purchased from AZ Electronic Materials.

Micromodel Fabrication. The micromodel was fabricated following a modified photolithography procedure (Figure 1S) in a class 10 clean-room.[1] A total of 9 micromodels was fabricated from one silicon wafer. The pore network pattern and Fe_2O_3 coating pattern (Figure 2S) were designed by AutoCAD (Autodesk) and transferred onto separate chrome masks (Fineline Imaging). The pore network pattern was etched into a silicon wafer following the procedures described in our previous publication.[1]

Briefly, as shown in Figure 1SA, the wafer was coated with a layer (8 μm thickness) of photoresist polymer (PR, AZ 4620). Then the pore network pattern on the mask was selectively exposed to ultraviolet (UV) light (EVGroup) for 25 s and the pattern was transferred to the wafer. PR exposed to UV light was removed by a PR developer (AZ 400K) as shown in Figure 1SB. The exposed area was etched to a depth around 25 μm using an inductively coupled plasma-deep reactive ion etching (ICP-DRIE) system (Plasmatherm). Then, the wafer was cleaned using a PR stripper (AZ 400 T), acid solution (H_2SO_4: H_2O_2 = 3:1), and SC1 solution (deionized water: H_2O_2: NH_4OH = 5:1:1) following our previous publication.[1] A layer of 0.15 μm silicon dioxide

was created on the silica wafer by thermal dry oxidation at 1100 °C for 1.5 hr. The pore network of the micromodel is shown in Figure 1SC.

For micromodel without the Fe_2O_3 coating, the inlet and outlet (0.8 mm in diameter） of the micromodel were drilled using a micro press drill (Micro Drill Presses) equipped with a 1 inch diameter diamond plated drill (UKAM Industrial). After being cleaned with oxygen plasma (March Plasma System) and SC1 solution, the silica wafer was sealed with a glass wafer and cut into separate micromodels as described in a previous publication.[1]

To fabricate the wafer with a patchwise charged heterogeneous surface, the etched and oxidized wafer was coated with another layer (8 μm thickness) of PR (Figure 1SD). Then a second mask (Figure 2S) was applied to selectively expose the area that will be coated with Fe_2O_3 (exposed under UV light for 50 s). The exposed area was transparent on the second mask. After exposed to UV light, the PR on the wall of the cylindrical collectors from top to bottom, and an area adjacent to the collectors was removed by the PR developer (Figure 1SE). As shown in Figure 1SF, the wafer was coated with 100 nm Fe_2O_3 in a magnetron sputtering deposition system (Discovery 785, Denton Vacuum Inc.). The wafer was then cleaned with PR stripper to remove the PR and unwanted Fe_2O_3 (Figure 1SG). At last, the wafer was drilled, cleaned, sealed and cut into separate micromodels as described above.

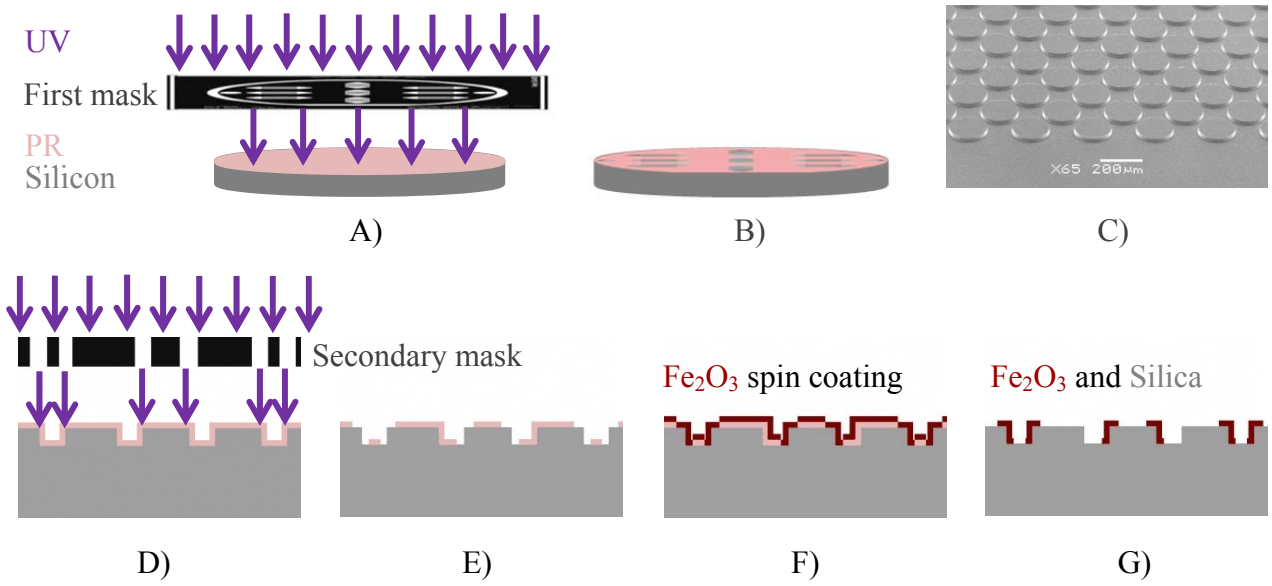

Figure 1S. Micromodel fabrication procedure. Grey: silicon or silica surface, Pink: photoresist (PR), Black: mask, Violet: UV light, and Red: Fe_2O_3 surface. Figures (A) and (B) are an illustration of the whole silicon wafer which had 9 micromodels. Figure (C) is the SEM (Scanning Electron Microscopy) picture of the inlet area of one micromodel. Figures (D), (E), (F), and (G) are the illustration of part of the pore network.

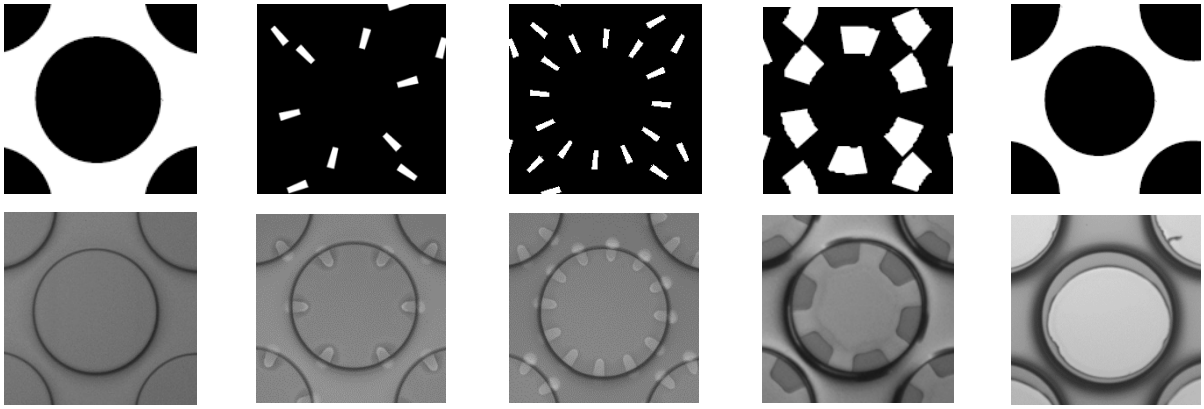

A) 0% B) 10% C) 20% D) 50% E) 100%

Figure 2S. Illustration of the masks and collectors. Transparent area on the mask (A) was etched into the silica wafer. Transparent area on the mask (B), (C), (D), and (E) was coated with Fe_2O_3. The width of the Fe_2O_3 band was 9.9, 9.9 and 49.7 μm for collectors coated with 10 (B), 20 (C), and 50% (D) Fe_2O_3.

Micromodel Characterization. Raman spectroscopy (Horiba Jobin Yvon Inc.) was used to confirm the crystal structure of Fe_2O_3 coated on the silica collector. Scanning electron microscopy (SEM) was used to characterize the structure of Fe_2O_3 coated and silica surfaces on the collector. Full elemental spectra were acquired for 4.5 × 3 μm area at more than 10 locations on Fe_2O_3 coated and silica surfaces separately by energy dispersive X-ray spectroscopy (EDS, FEI XL30 ESEM-FEG microscopy) to evaluate the quality of Fe_2O_3 coating. The SEM and EDS were operated at accelerating voltage (Acc.V) of 5.0 kV and 15.0 kV, respectively.

***C. parvum* Oocyst Preparation**. *C. parvum* oocysts (4-5 μm in diameter) were propagated using an infected male Holstein calf. The procedure was complied with protocols approved by the University of Illinois Institutional Animal Care and Use Committee. The feces were collected and oocysts were purified following a previously published protocol.[2] A mixture of Hanks' balanced salt and antibiotic-antimycotic solution was used to store oocysts at 4°C.

Fourier Transform Infrared Spectroscopic (FT-IR) Imaging. Infrared spectroscopic imaging data were acquired using a Perkin Elmer Spotlight 400 imaging system (Perkin Elmer, Waltham, MA). FT-IR images were acquired in the attenuated total reflectance (ATR) imaging mode using a Germanium crystal ATR imaging adapter. A drop of highly concentrated oocysts was placed on a FTIR crystal adapter to form oocyst layers. Data were collected across the nominal free-scanning spectral range and saved over 4000–750 cm^{-1}, and were recorded with an interferometer speed of 1.0 cm/s and collected using a linear mercuric cadmium telluride (MCT)

detector array. Spectral images were acquired with a pixel size of 1.56 μm × 1.56 μm, with 4 scans per pixel at a spectral resolution of 4 cm^{-1}. ATR images were acquired across a 100 μm × 100 μm region of the ATR crystal. The ATR crystal was gently placed in contact with the sample using minimal pressure to ensure good contact and minimize sample damage. All data were exported to the program ENVI/IDL and all computation was performed using in-house written programs.

Hamaker Constant. The Hamaker constant of oocyst-water-silica system (1.2×10^{-21} J) was reported in our previous publication.[3] The Hamaker constant of oocyst-water-Fe_2O_3, carboxylate microsphere-water-silica and carboxylate microsphere-water-Fe_2O_3 systems was determined from Lifshitz-van der Waals (LW) component of surface energy (γ^{LW}) as described in the previous publication.

$$A = -12\pi y_0^2 \Delta G_{y0}^{LW} \tag{1}$$

$$\Delta G_{y0}^{LW} = 2\left(\gamma_l^{LW} - \gamma_s^{LW}\right)\left(\gamma_c^{LW} - \gamma_l^{LW}\right) \tag{2}$$

where y_0 is minimum equilibrium cut-off distance[4] that is usually assigned a value of 0.157 nm, ΔG_{y0}^{LW} is LW component of free energy of adhesion, γ_c^{LW} is γ^{LW} of oocysts or carboxylate microspheres, γ_l^{LW} is γ^{LW} of water, and γ_s^{LW} is γ^{LW} of silica or Fe_2O_3. The values of ΔG_{y0}^{LW} and γ^{LW} were reported in the literature.[3-6]

Table 1S. Surface energy ($\gamma^{LW}, \Delta G_{y0}^{LW}$) and Hamaker constant ($A$) in the presence of water at 20℃

	γ^{LW}/ΔG_{y0}^{LW} (mJ/m^2)	A(J)
Water	21.8 [a, c]	
Oocysts	26.9 [a, d]	
Carboxylate microspheres	31.4 [a, e]	
Silica (Quartz)	35.6 [a, d]	
Fe_2O_3 (Hematite)	48.5 [a, f]	
Oocyst-water-silica	-1.33 [b]	1.2×10^{-21}
Oocyst-water-Fe_2O_3	-2.16 [b]	2.2×10^{-21}
Carboxylate microsphere-water-silica	-2.42 [b]	2.2×10^{-21}
Carboxylate microsphere-water-Fe_2O_3	-3.92 [b]	4.0×10^{-21}

[a] γ^{LW}: LW component of surface tension

[b] ΔG_{y0}^{LW}: LW component of free energy of adhesion per unit area

[c] Data from van Oss[4]

[d] Data from Liu et al.[3]

[e] Data from Janjaroen et al.[5]

[f] Data from Plaze et al.[6]

Micromodel Setup. The micromodel was assembled on a stainless steel manifold equipped with Teflon FEP tubing (0.18 mm inner diameter, Upchurch) as shown in Figure 3S. Then the manifold was mounted on a microscope (Leica, DMI5000 M) with a reflected differential interference contrast (DIC) and a FITC filter. The micromodel was saturated with colloid free electrolytes, before oocysts or microspheres were pumped into it, at a constant volumetric flow rate, corresponding to an average linear velocity in the pore network of 1.86 mm/s. This is close to the lowest velocity that the syringe pump can deliver colloids reliably and that a substantial number of oocysts can be pumped into the micromodel without sticking to the wall of the Teflon tubing. Auset and Keller[7] reported that colloid attachment decreased less than 2 times when the flow velocity increased more than 20 times (from 0.05 to 1 mm/s). Though the flow velocity used in our system was rather high compared with natural groundwater, we would expect that the attachment mechanisms investigated in this study will be valid at lower flow rate as well.

The colloid concentration ranged from 0.5×10^6 to 1.5×10^6 particles/mL. Lower colloid concentration was selected for attachment at favorable conditions (i.e., attachment on silica collectors at lower pH or on collectors coated with Fe_2O_3) so that colloid-collector interaction was dominant at the initial stage of attachment. Higher colloid concentration was selected for attachment at unfavorable conditions (i.e., attachment on silica collectors at higher pH) so that there was detectable oocyst attachment on the collectors. The colloid solution was kept suspended using a magnetic stirrer during the course of the experiment (i.e., 2-90 min). The

colloid concentrations were low and in a narrow range that no aggregation occurred and the colloid input concentration would not significantly affect the colloid attachment in this study.[8]

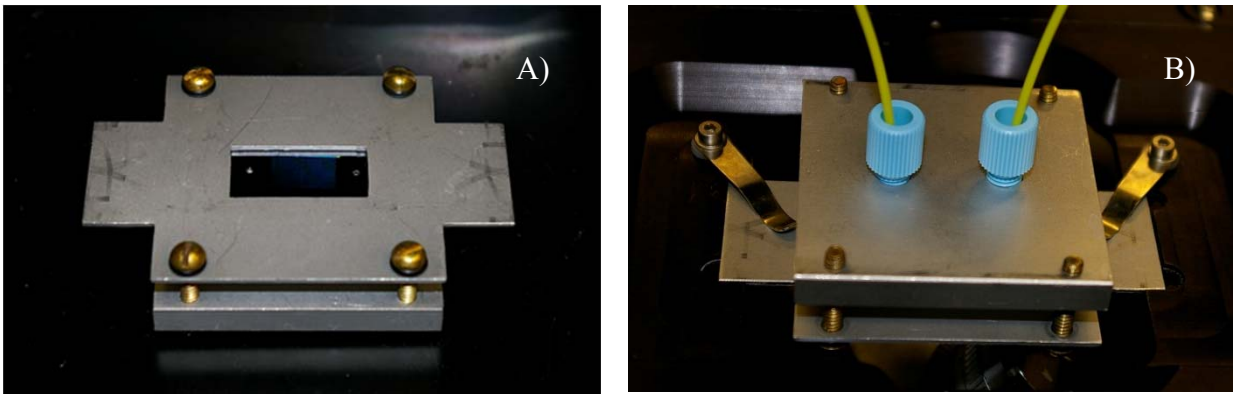

Figure 3S. (A) A micromodel was assembled on a manifold and (B) the manifold was mounted on the stage of a microscope.

Calculation of Average Removal Efficiency and Attachment Efficiency. The average single collector removal efficiency (η) was calculated as the ratio of the average number of colloids attached to one collector over the number of colloids approaching the projected area of one collector.[7, 9] The equation was modified from previous publication.[9] Since the collectors used in our work are cylindrical collectors instead of spherical collectors, the projected area in our work should be $D \times d_c$ instead of $\pi \times a_c^2$.

$$\eta = \frac{I}{Dd_c uC_0} \tag{3}$$

where I is an average attachment rate of oocysts on one cylindrical collector (I is obtained by dividing the total number of attached oocysts by the product of experimental duration time and the number of collectors), D is the height of the cylinder, d_c is the diameter of the cylinder, u is the Darcy velocity, and C_0 is the oocyst concentration.

The average removal efficiencies for only Fe_2O_3 patches ($\eta_{Fe_2O_3}$) and only silica patches (η_{silica}) were calculated as the ratios of the number of colloids attached to the Fe_2O_3 patches or the silica patches over the number of colloids approaching the patches on the collectors.

$$\eta_{Fe_2O_3} = \frac{I_{Fe_2O_3}}{Dd_c uC_0 \lambda} \tag{4}$$

$$\eta_{silica} = \frac{I_{silica}}{Dd_c uC_0 (1-\lambda)} \tag{5}$$

where $I_{Fe_2O_3}$ and I_{silica} are average attachment rate of oocysts on Fe_2O_3 patches or on silica patches, respectively, and λ is the fraction of Fe_2O_3 surface.

The average attachment efficiency (α) of colloids was determined by the ratio between the average single collector removal efficiencies (η, η_{total} on collectors coated with 0, 10, 20, 50, or 100% Fe_2O_3) and the maximum average single collector removal efficiencies for favorable conditions (η_0).

$$\alpha = \frac{\eta}{\eta_0} \tag{6}$$

Microsphere Attachment Observed with Confocal Microscopy. The vertical distribution of microspheres attached to a charged heterogeneous collector wall at 1 mM NaCl, pH 7.1 ± 0.1, and buffered with 0.05 mM $NaHCO_3$ was determined using a laser scanning confocal microscopy (Zeiss LSM 710 Upright) to study the role of sedimentation in the charged heterogeneous micromodel and the influence of the adjacent Fe_2O_3 surface at the bottom of the micromodel. This experiment was conducted with microsphere instead of oocysts because viable oocysts were not allowed in the lab housing the confocal microscope. Due to the limited access to the confocal microscope and because the purpose of this experiment was not relevant to solution pH, a pH (pH 7.0) that is close to the isoelectric point of Fe_2O_3 and in the middle of the studied pH was selected. The micromodel was installed on a confocal microscope with a 40 × magnification water immersion objective. The fluorescence of microspheres was excited by an argon ion gas laser at 488 nm. The confocal pinhole size of 1.5 airy disk, which resulted in 1.7 μm of optical section resolution, was set to eliminate light that is out of the focal plane. The fluorescence images were scanned with every 1 μm Z section from the bottom of the pore

network to the top of the collectors. Each image was converted to a binary image by setting a threshold of 40 using ImageJ. In the binary image, pixels with a grey value above the threshold were marked as “object” pixels (fluorescent signal pixels of microsphere) and pixels with a grey value below the threshold were marked as “background” pixels. The total number of “object” pixels on all the pictures were summed up and divided by the total number of microspheres to determine the total pixels of a single microsphere. Then the number of “object” pixels on each binary image was normalized by the total intensity of a single microsphere (i.e., sum of pixel intensity of one microsphere) to investigate the distribution of the attached microspheres on the collector wall.

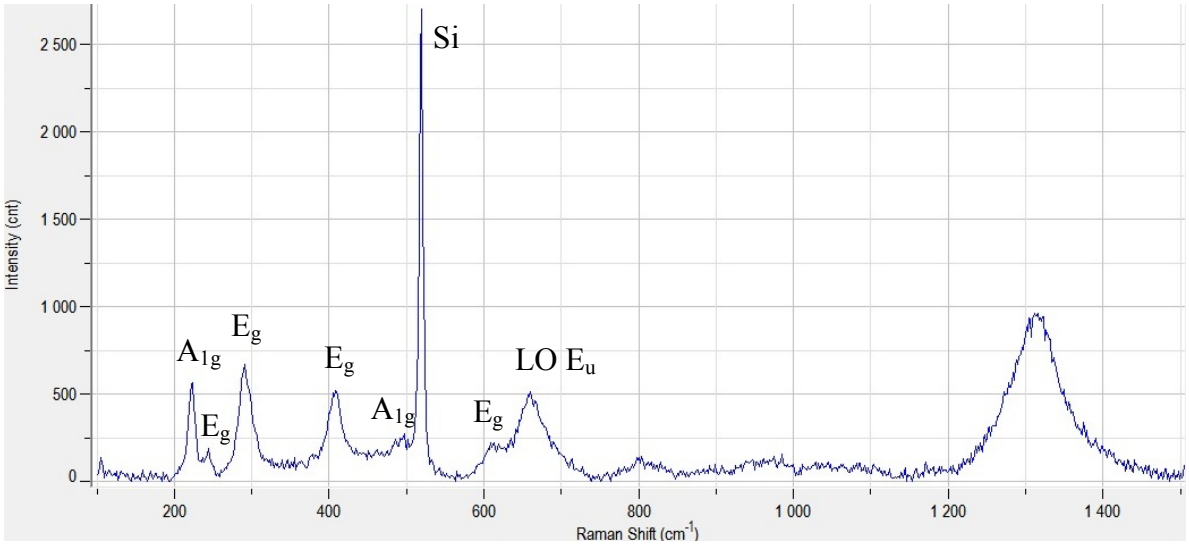

Figure 4S. Raman spectra of thin Fe_2O_3 film coated on silica surface. Raman shift (cm^{-1}) assigned to hematite: 229 (A_{1g}), 249 (E_g), 295 (E_g), 414 (E_g), 500 (A_{1g}), 615 (E_g), and 660 (LO E_u)[10] and to silica: 520[11].

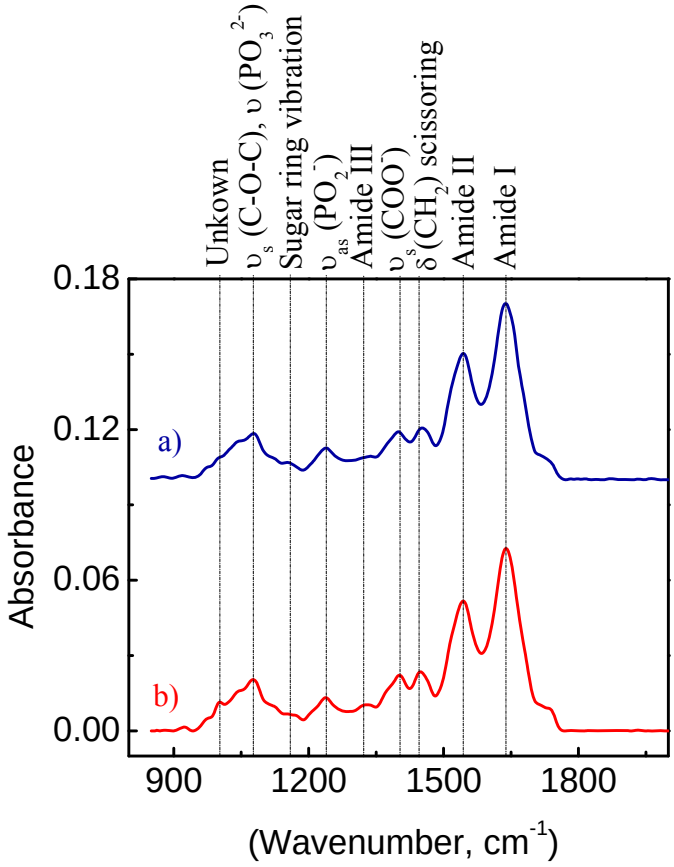

Figure 5S. FT-IR spectra of viable oocyst suspension scanned at different locations in deionized water at pH 5.7-5.9. The deionized water background was subtracted from the spectra. Amide I: C=O, C-N, N-H, amide II: N-H, C-N, and amide III: N-H, C-N, C-H, N-H.

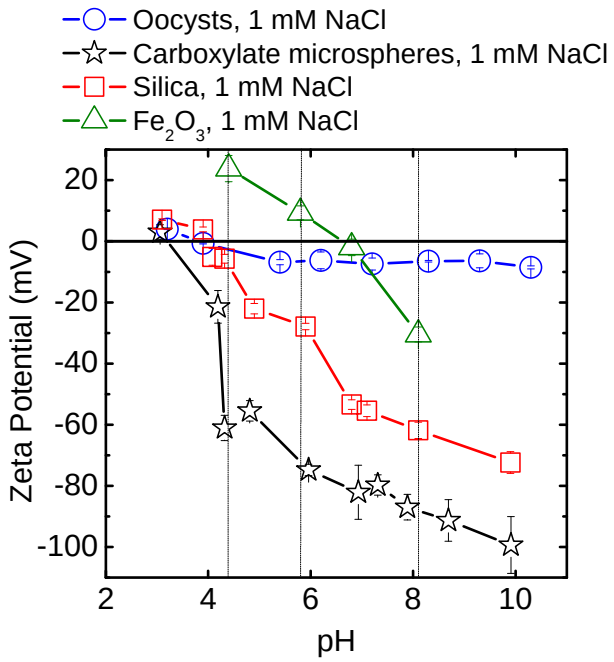

Figure 6S. Zeta potential of oocysts, microspheres, pulverized silica, and pulverized Fe_2O_3 particles at 1 mM NaCl as a function of pH in 1 mM NaCl.

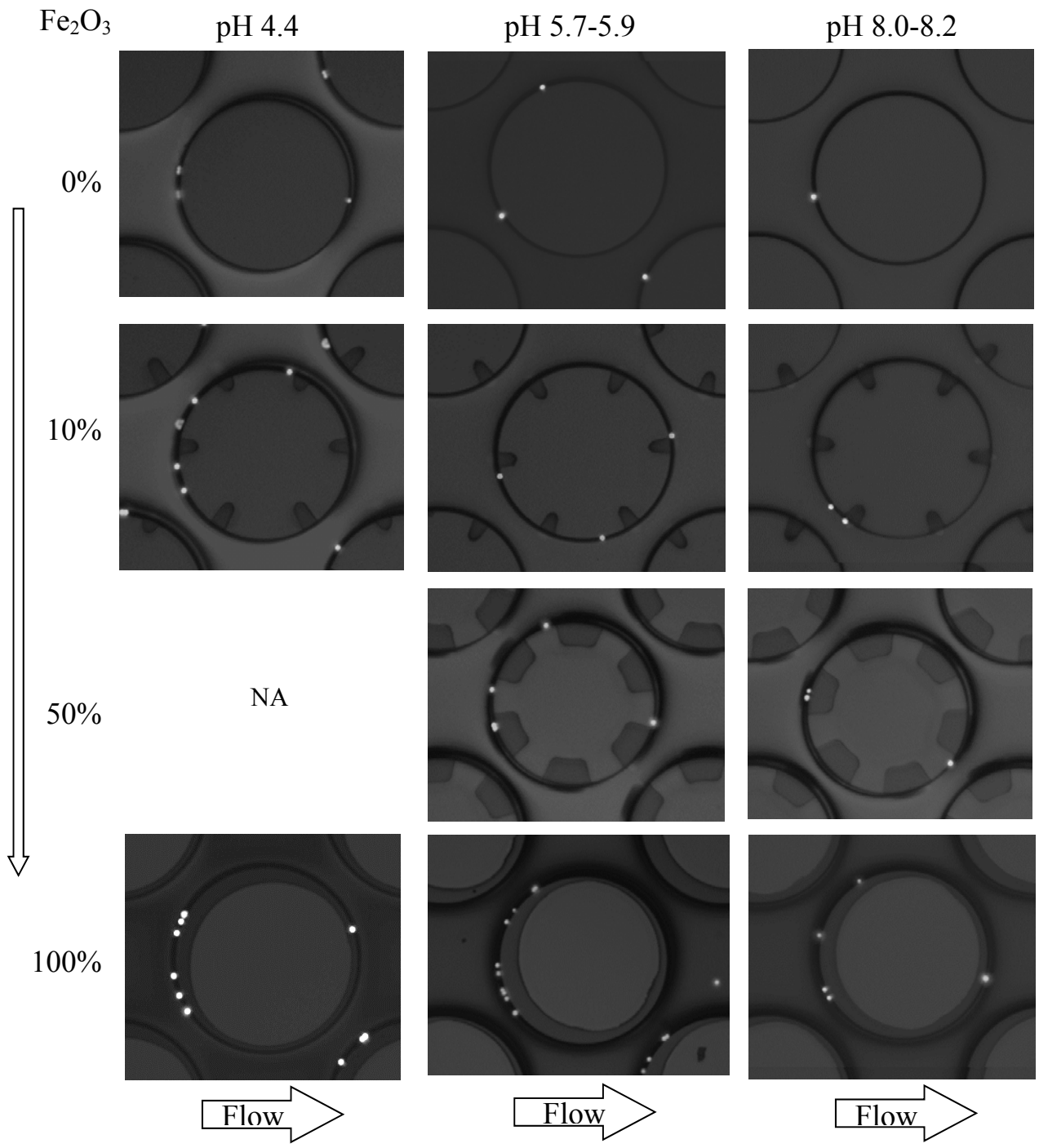

Figure 7S. Attachment of carboxylate microspheres on silica collectors coated with 0, 10, 50, and 100% Fe_2O_3. Experimental solution chemistry: 1 mM NaCl at pH 4.4, 1 mM NaCl at pH 5.8, or 1 mM $NaHCO_3$ at pH 8.1. Linear velocity = 1.86 mm/s.

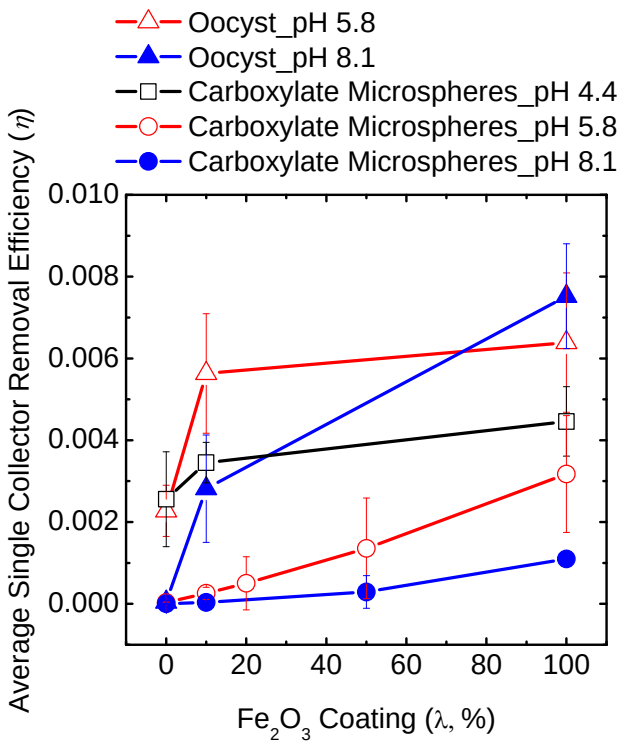

Figure 8S. Average single collector removal efficiency (η_{total}) of oocysts (triangle) and carboxylate microspheres (square and circle) on silica collectors coated with 0, 10, 20, 50, and 100% Fe_2O_3. Experimental solution chemistry: 1 mM NaCl at pH 4.4 (black), 1 mM NaCl at pH 5.8 (red), or 1 mM $NaHCO_3$ at pH 8.1 (blue). Linear velocity = 1.86 mm/s.

Literature Cited

1. Liu, Y.; Zhang, C.; Hilpert, M.; Kuhlenschmidt, M. S.; Kuhlenschmidt, T. B.; Nguyen, T. H. Transport of *Cryptosporidium* parvum oocysts in a silicon micromodel. *Environmental Science & Technology* **2012,** *46* (3), 1471-1479.
2. Johnson, J. K.; Schmidt, J.; Gelberg, H. B.; Kuhlenschmidt, M. S. Microbial adhesion of *Cryptosporidium parvum* sporozoites: Purification of an inhibitory lipid from bovine mucosa. *Journal of Parasitology* **2004,** *90* (5), 980-990.
3. Liu, Y.; Kuhlenschmidt, M. S.; Kuhlenschmidt, T. B.; Nguyen, T. H. Composition and conformation of *Cryptosporidium parvum* oocyst wall surface macromolecules and their effect on adhesion kinetics of oocysts on quartz surface. *Biomacromolecules* **2010,** *11* (8), 2109-2115.
4. van Oss, C. J. Acid--base interfacial interactions in aqueous media. *Colloids and Surfaces a-Physicochemical and Engineering Aspects* **1993,** *78*, 1-49.
5. Janjaroen, D.; Ling, F.; Monroy, G.; Derlon, N.; Mogenroth, E.; Boppart, S. A.; Liu, W.-T.; Nguyen, T. H. Roles of ionic strength and biofilm roughness on deposition kinetics of *Escherichia coli* onto groundwater biofilm grown on PVC surfaces. *Water Research* **2012,** *Submitted*.
6. Plaza, R. C.; Zurita, L.; Durán, J. D. G.; González-Caballero, F.; Delgado, A. V. Surface thermodynamics of hematite/yttrium oxide core−shell colloidal particles. *Langmuir* **1998,** *14* (24), 6850-6854.
7. Auset, M.; Keller, A. A. Pore-scale visualization of colloid straining and filtration in saturated porous media using micromodels. *Water Resources Research* **2006,** *42* (12).
8. Haznedaroglu, B. Z.; Kim, H. N.; Bradford, S. A.; Walker, S. L. Relative transport behavior of *Escherichia coli* O157:H7 and *Salmonella enterica* serovar pullorum in packed bed column systems: influence of solution chemistry and cell concentration. *Environmental Science & Technology* **2009,** *43* (6), 1838-1844.
9. Tufenkji, N.; Elimelech, M. Correlation equation for predicting single-collector efficiency in physicochemical filtration in saturated porous media. *Environmental Science & Technology* **2004,** *38* (2), 529-536.
10. Jubb, A. M.; Allen, H. C. Vibrational spectroscopic characterization of hematite, maghemite, and magnetite thin films produced by vapor deposition. *ACS Applied Materials & Interfaces* **2010,** *2* (10), 2804-2812.
11. Piscanec, S.; Ferrari, A. C.; Cantoro, M.; Hofmann, S.; Zapien, J. A.; Lifshitz, Y.; Lee, S. T.; Robertson, J. Raman spectrum of silicon nanowires. *Materials Science and Engineering C* **2003,** *23*, 931-934.